

# LSGQuant: Layer-Sensitivity Guided Quantization for One-Step Diffusion Real-World Video Super-Resolution

Tianxing Wu\*<sup>1</sup> Zheng Chen\*<sup>1</sup> Cirou Xu<sup>1</sup> Bowen Chai<sup>1</sup> Yong Guo<sup>2</sup>  
 Yutong Liu<sup>1</sup> Linghe Kong<sup>1</sup> Yulun Zhang<sup>† 1</sup>

## Abstract

One-Step Diffusion Models have demonstrated promising capability and fast inference in video super-resolution (VSR) for real-world. Nevertheless, the substantial model size and high computational cost of Diffusion Transformers (DiTs) limit downstream applications. While low-bit quantization is a common approach for model compression, the effectiveness of quantized models is challenged by the high dynamic range of input latent and diverse layer behaviors. To deal with these challenges, we introduce LSGQuant, a layer-sensitivity guided quantizing approach for one-step diffusion-based real-world VSR. Our method incorporates a Dynamic Range Adaptive Quantizer (DRAQ) to fit video token activations. Furthermore, we estimate layer sensitivity and implement a Variance-Oriented Layer Training Strategy (VOLTS) by analyzing layer-wise statistics in calibration. We also introduce Quantization-Aware Optimization (QAO) to jointly refine the quantized branch and a retained high-precision branch. Extensive experiments demonstrate that our method has nearly performance to origin model with full-precision and significantly exceeds existing quantization techniques. All models and code are available at <https://github.com/zhengchen1999/LSGQuant>.

## 1. Introduction

As an essential and important computer vision task, video super-resolution (VSR) tries to reproduce high-quality videos with origin low-quality counterparts. With the fast promotion of smartphone video capture technologies and the widespread adoption of video streaming platforms, VSR has gained growing significance in practical applications. Initial VSR approaches (Jo et al., 2018; Nah et al., 2019; Liang et al., 2024) mainly concentrate on synthetic degra-



Figure 1. Low-bit LSGQuant comparison with bfloat16 full-precision model, the recent leading quantization methods ViDiT-Q (Zhao et al., 2025) and SVDQuant (Li et al., 2025a).

dation scenarios, where low-resolution (LR) videos are produced using degradation assumptions like down-sampling. Nevertheless, such methods perform poorly in real-world environments with complex and unknown degradations.

To tackle these issues, a variety of approaches have been developed for real-world VSR. Among them, diffusion models can generate visually realistic details while maintaining stable training behavior (Ho et al., 2020; Blattmann et al., 2023; Zhou et al., 2024; Yang et al., 2025; Xie et al., 2025). Despite these advantages, DMs have high inference costs because of iterative denoising procedures. Although single-step diffusion models demonstrate strong ability in visual super-resolution (Chen et al., 2025; Wang et al., 2025), these models remain computationally heavy due to large-scale backbone architectures. Consequently, the inference cost of one-step diffusion VSR models is still relatively high, which restricts their real-world applicability.

Low-bit quantization serves as an effective approach to further lowering inference costs, due to its ability to significantly decrease computation costs. Through transferring floating-point values into low-precision, quantization facilitates model deployment on edge devices or platforms which have limited resources. However, applying low-bit quantization to diffusion-based video super-resolution models remains highly challenging. First, aggressive low-bit quantization often leads to severe performance degradation and noticeable loss in generation quality, particularly in video settings. Second, minimizing the quantization error during optimization often leads to overfitting the low-bit representation instead of optimal VSR performance.

\*Equal contribution <sup>1</sup>Shanghai Jiao Tong University <sup>2</sup>Huawei.  
 Correspondence to: Yulun Zhang <yulun100@gmail.com>.

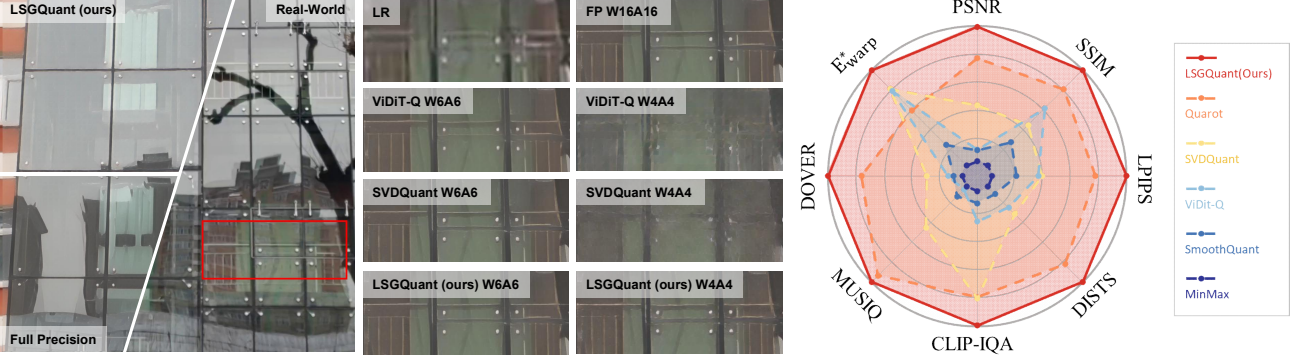


Figure 2. Performance comparisons on the synthetic REDS30 dataset (Nah et al., 2019) between different quantization methods in 4-bit and 6-bit scenarios. LSGQuant achieves leading scores on all evaluation metrics.

Motivated by these challenges, we propose LSGQuant, a layer-sensitivity guided quantization framework for one-step diffusion real-world VSR. We select the prominent text-to-video (T2V) model WAN2.1 (Wan et al., 2025) as a full precision (FP) backbone, and adopt training settings of DOVE (Chen et al., 2025) for one-step diffusion VSR tasks. We apply several common methods in low-bit quantization, including Hadamard rotation (Ashkboos et al., 2024) and high-precision branch (Li et al., 2025a). Three novel components are introduced to address the specific challenges outlined earlier. Firstly, to handle the varying range, we introduce a Dynamic Range Adaptive Quantizer (DRAQ) to minimize quantization error. Second, our Variance-Oriented Layer Training Strategy (VOLTS) dynamically allocates training resources by re-estimating layer sensitivity, thereby enhancing output fidelity. Finally, we employ a Quantization-Aware Alternating Optimization (QAO) algorithm to refine quantized and full-precision branches.

Extensive experiments (*i.e.*, Figs 1 and 2) show that, under 4-bit quantization, LSGQuant has only negligible performance degradation and surpasses recent state-of-the-art quantization settings. When competing with the bfloat16 model, 4-bit LSGQuant achieves reductions of 70.49% in parameters (Params) and 71.92% in operations (Ops).

We list our contribution as follows:

- We introduce LSGQuant, an approach for one-step diffusion-based real-world VSR in model quantization. To the best of our knowledge, our approach firstly investigates low-bit(*e.g.*, 4-bit) scenario.
- We design a Dynamic Range Adaptive Quantizer (DRAQ) that effectively addresses the quantization error in the quantized inference process.
- In the calibration process, our Variance-Oriented Layer Training Strategy (VOLTS) and Quantization-Aware Alternating Optimization (QAO) provide reliable layer sensitivity estimation and quantization.

- Evaluations raised on both real-world and synthetic datasets demonstrate advantageous behavior of our approach over existing quantization settings.

## 2. Related Work

### 2.1. Video Super-Resolution

Video super-resolution (VSR) originates from entering low visual quality videos to get its high-resolution (HR) counterparts. Primitive VSR approaches (Jo et al., 2018; Chan et al., 2021; Liang et al., 2024) have achieved impressive performance. To better deal with unfixed degradation assumptions in the real-world, suitable datasets and model architecture are mainly focused on. To construct more realistic datasets, RealBasicVSR (Chan et al., 2022) introduce diverse degradation models to synthesize training data, while MVS4x (Wang et al., 2023b) collected LR-HR paired data from real environments. Besides, several real-world VSR methods enhance reconstruction quality by incorporating specialized architectural components. DiffVSR (Li et al., 2025b) imports multi-scale temporal attention for capturing temporal dependencies. Despite these significant advances, methods still have flaws in generating textures and details.

### 2.2. Diffusion Model

Diffusion models gain success in multiple computer tasks across both image (Ho et al., 2020; Ramesh et al., 2022; Rombach et al., 2022) and video (Blattmann et al., 2023; Chen et al., 2024; Zhou et al., 2024; Yang et al., 2025; Li et al., 2025b; Xie et al., 2025; Wang et al., 2025) visual domains. To accelerate inference speed, one-step diffusion has been proposed as an extreme acceleration paradigm by decreasing inference steps from multi-step into 1. OSEDiff (Wu et al., 2024b) introduces one-step diffusion into image super-resolution via variational score distillation (Wang et al., 2023c), while DOVE (Chen et al., 2025) adopts high-quality fine-tuning with a latent-pixel strategy to adapt one-step diffusion models to video super-resolution. Despite

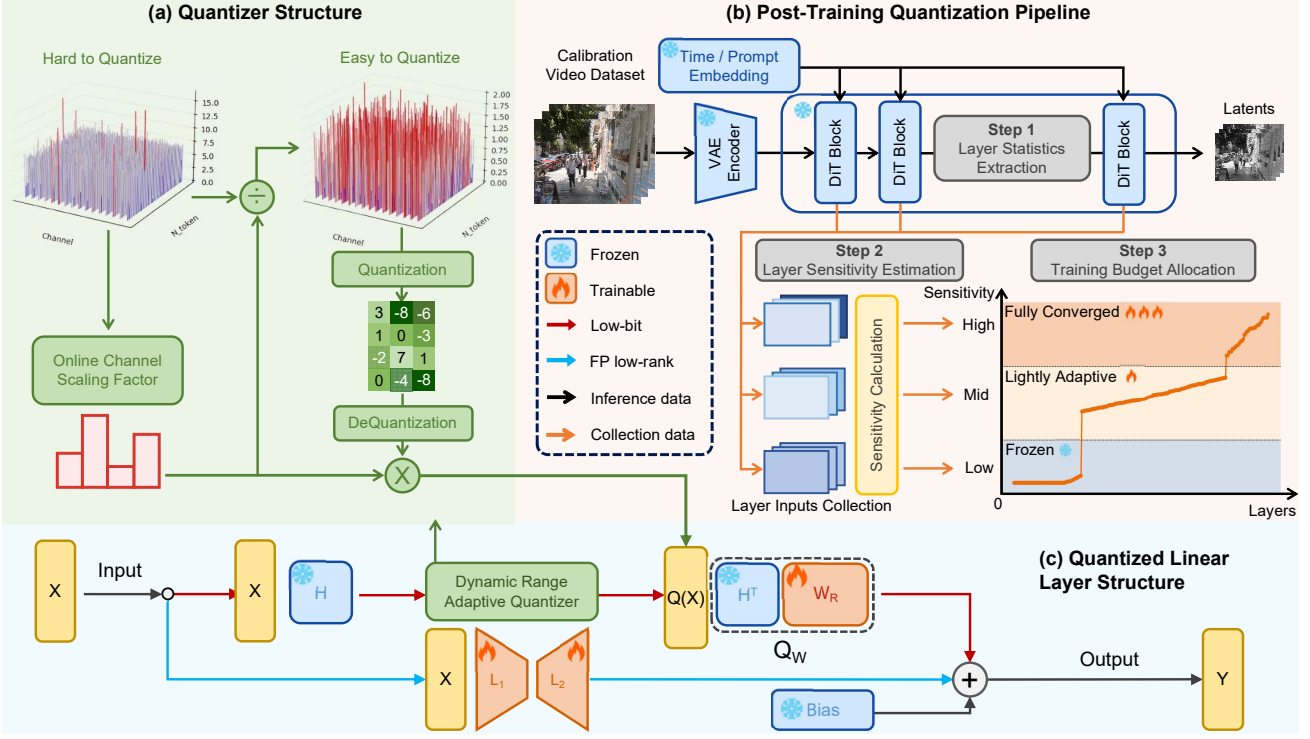


Figure 3. Overview of our LSGQuant. **Firstly**, we collect per-channel layer statistics by a single inference process. **Next**, we calculate layer sensitivity and estimate its importance to the final video output. **Finally**, we allocate training iterations by estimated sensitivities.

significant speedup, one-step diffusion models remain computationally intensive due to large-scale architectures such as U-Net or Diffusion Transformer (DiTs).

### 2.3. Model Quantization

Model Quantization (Jacob et al., 2018) is a widespread lightning skill for neural network compression, aiming to reduce computational cost and memory footprint by representing floating-point values with low-bit numerical formats. To reduce the impact of outliers on quantization accuracy, equivalent transformation are widely used for reconciling quantization difficulty between activation and weights. SmoothQuant (Xiao et al., 2023) migrates activation outliers into weights through offline scaling, while QuaRot (Ashkboos et al., 2024) removes hidden-state outliers via Hadamard rotations. Recent studies have also explored quantization for diffusion models. SVDQuant (Li et al., 2025a) proposes a high-precision but low rank and computation cost branch to compensate quantization errors. The additional branch clearly fill the precision gap brought by quantization. Additionally, some quantization methods are designed for specific tasks, such as ViDiT-Q (Zhao et al., 2025) for visual generation and PassionSR (Zhu et al., 2025) for image super-resolution. Nevertheless, existing quantization models exhibit unsatisfactory performance when applied to video super-resolution based on one-step models.

## 3. Methodology

Our proposed LSGQuant will be fully introduced in this section, as shown in Fig. 3. First, we give preliminaries about quantization. Then, we describe our overall architecture for quantization layers and framework for post-training quantization (PTQ) process. Finally, we give motivation and implementations for proposed methods, *i.e.*, Dynamic Range Adaptive Activation Quantizer (DRAQ), Variance-Oriented Layer Training Strategy (VOLTS), and Quantization-Aware Alternating Optimization (QAO).

### 3.1. Preliminaries

**Model quantization** reduces computational and memory footprints by using low-bit integer to replace floating-point, accompanied by high-bit parameters for efficiency. Given an input floating-point value  $x$ , the quantization and inverse procedures can be formally expressed as:

$$x_{int} = \text{Clip}(\lfloor \frac{x}{s} \rfloor - z, l, u), \hat{x} = s \cdot (x_{int} + z), \quad (1)$$

where  $x_{int}$  is the quantized integer value bounded by the clip boundary  $l$  and  $u$ , which are determined by the quantization bit-width and symmetric type.  $s$  and  $z$  denotes scaling factors and zero points respectively.

**Pre-scaling-based methods** (Xiao et al., 2023; Wu et al., 2024a; Zhao et al., 2025) uses a channel-wise scaling factor

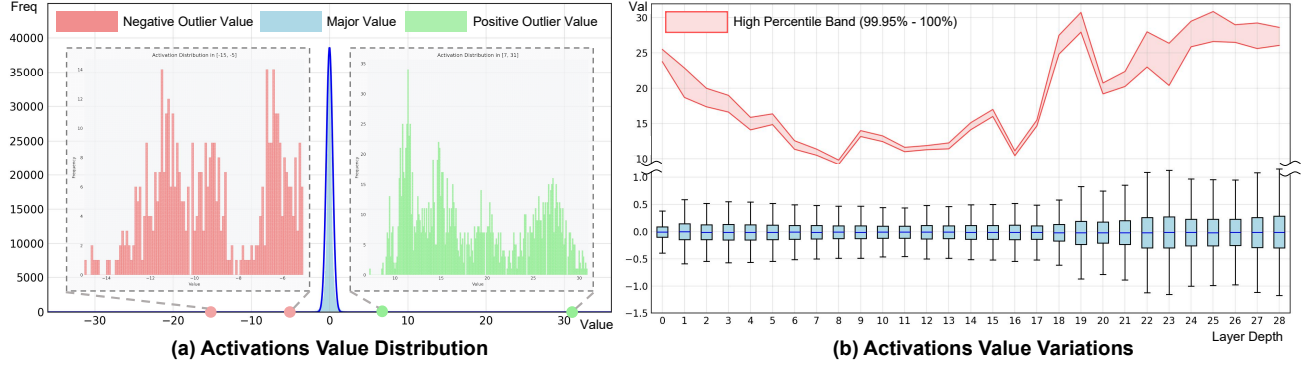


Figure 4. Input data sampled from cross-attention query layer. (a) Statistical distribution of activation values. While majority of values are concentrated near zero, a significant long-tail distribution exists. These extreme values would dominate the quantization range. (b) Distribution of input latent values across different blocks. The statistical characteristics of outliers varies with depth.

$s \in \mathbb{R}^c$  to migrates activation outliers into weights:

$$s_i = \frac{\max(|\mathbf{X}_{:,i}|)^\alpha}{\max(|\mathbf{W}_{:,i}|)^{1-\alpha}}, i \in \{1, 2, \dots, C\},$$

$$\mathbf{s} = \text{diag}(s_1, s_2, \dots, s_C),$$

$$\mathbf{Y} = \mathbf{Q}_A(\mathbf{X}\mathbf{s}^{-1}) \cdot \mathbf{Q}_W(\mathbf{s}\mathbf{W}) + \mathbf{b},$$
(2)

where  $C$  is used as input channel number, and  $\alpha$  is a hyperparameter used to control the degree of outlier transfer. This parameter can be finetuned on the calibration dataset, or simply set to a uniform value across all layers.

**Rotation-based methods** (Ashkboos et al., 2024; Liu et al., 2025; Zhao et al., 2025) employs rotation matrix  $\mathbf{Q}$  which satisfies  $\mathbf{Q}\mathbf{Q}^T = \mathbf{I}$  and  $|\mathbf{Q}| = \mathbf{I}$ .  $\mathbf{Q}$  can be generated by fast-hadamard-transform or trained on manifold. By respectively applying  $\mathbf{Q}$  and  $\mathbf{Q}^T$  on weights and activations, large outliers are effectively suppressed.

### 3.2. Overall Framework

LSGQuant adopt WAN2.1 (Wan et al., 2025), a multi-step diffusion model, as the backbone network. Following settings same with DOVE (Chen et al., 2025), we train a one-step version for VSR tasks. The diffusion transformer (DiT) module dominates the computational costs in inference process, so we focus on quantizing all linear modules in DiT by replacing original layers with quantized layers.

The whole architecture of the quantization layer is shown in Fig 3(c). The layer has two main branches, include a low-bit quantized branch and a full-precision (FP) low-rank branch. The entire formulation for layer is:

$$\mathbf{Y} = \mathbf{X}\mathbf{W} + \mathbf{b} \approx \underbrace{\mathbf{X}\mathbf{L}_1\mathbf{L}_2}_{\text{FP, low-rank}} + \underbrace{\mathbf{Q}_A(\mathbf{X}\mathbf{H})\mathbf{Q}_W(\mathbf{H}\mathbf{W})}_{\text{low-bit quantized}} + \mathbf{b}.$$
(3)

In the full-precision and low-rank branch, we apply two matrices  $\mathbf{L}_1 \in \mathbb{R}^{m \times r}$  and  $\mathbf{L}_2 \in \mathbb{R}^{r \times n}$  for limiting computational costs. In the low-bit branch,  $\mathbf{Q}_W$  and  $\mathbf{Q}_A$  refers to different quantizer for weights and activation values, and  $\mathbf{W}_R = \mathbf{W} - \mathbf{L}_1\mathbf{L}_2$  to assure residual acts relatively comple-

mentation with the other branch. Following previous work,  $\mathbf{H}$  is the random Hadamard matrix, and applying these matrices can be computed through fast-hadamard-transform.

The calibration process comprises two important stages. Firstly, we analyze the layer sensitivity on the calibration dataset. We run a full inference process, collect layer statistics and allocate different training importance. Secondly, for each linear layer, we run the adaptive optimizing algorithm with different epoches decided in the last step. After the optimization, we confirm required parameters for  $\mathbf{L}_1$ ,  $\mathbf{L}_2$  and  $\mathbf{W}_R$  used for quantization inference process.

### 3.3. Dynamic-Range Adaptive Activation Quantizer

Activation distributions in Diffusion Transformers (DiTs) exhibit significant channel-wise imbalance. As illustrated in Fig. 4(a), a small number of channels contain extreme outlier values that dominate the overall quantization range. Consequently, conventional min-max quantization suffers from severe resolution loss, especially under low-bit (e.g., 4-bit) constraints. Pre-scaling methods also face challenges because calibration datasets may not capture the full dynamic range of activations encountered during inference, leading to persistent quantization errors. Furthermore, quantization strategies designed for multi-step denoising can optimize migration degree  $\alpha$  by aggregating statistics across timesteps. However, this approach is ineffective for one-step inference, where activations are generated from single timestep and cannot be smoothed through temporal averaging.

To overcome these challenges, we propose the **Dynamic-Range Adaptive Activation Quantizer (DRAQ)**. For an activation tensor  $X_{N \times C}$ , which represents token numbers  $\times$  channel dimension, we first compute the channel-wise maximum absolute value  $S$  across all tokens, which provides a robust estimate of the per-channel dynamic range. Activations are then normalized by these estimated scales to the interval  $[-1, 1]$ . This normalization is friendly for symmetric quantization and suppresses outliers from a token-wise

perspective. Finally, the quantized values are rescaled to the original range, ensuring compatibility with subsequent layers and subsequent calculations.

As shown in Fig. 3(a), the whole quantization process can be formulated as follows:

$$\begin{aligned} s_i &= \max_N |\mathbf{X}_{N,i}|, \mathbf{s} = \text{diag}(s_1, \dots, s_C), \\ \tilde{\mathbf{X}} &= \mathbf{X}\mathbf{s}^{-1}, d_i = \max_C |\tilde{\mathbf{X}}_{i,C}|, \mathbf{d} = \text{diag}(d_1, \dots, d_N), \\ \hat{\mathbf{X}} &= \mathbf{d} \text{ Clamp} \left( \left[ (2^{n-1} - 1) \mathbf{d}^{-1} \tilde{\mathbf{X}} \right], -2^{n-1}, 2^{n-1} - 1 \right) \mathbf{s}, \end{aligned} \quad (4)$$

where  $n$  denotes the quantization bitwidth,  $\tilde{\mathbf{X}}$  and  $\hat{\mathbf{X}}$  denotes the scaled input  $\mathbf{X}$  and quantized  $\mathbf{X}$  respectively.

The scaling factors are computed online with negligible extra computational and memory costs. By normalizing activations with respect to their channel-wise maximum magnitudes, DRAQ directly adapts the quantization range to the activation statistics and aligns the effective dynamic ranges across channels, so that reducing quantization errors.

### 3.4. Variance-Oriented Layer Training Strategy

Existing quantization methods for Diffusion Transformers (DiTs) are designed for multi-step denoising (Shang et al., 2023; He et al., 2024; Zhao et al., 2025) and assume that all network layers contribute equally to output quality. This assumption becomes invalid for one-step diffusion models, where the entire latent output is generated in a single forward pass with a fixed timestep, and there is no opportunity for iterative steps to correct quantization errors.

Furthermore, one-step diffusion models are typically initialized and finetuned from large pretrained diffusion models (Wang et al., 2024; Dong et al., 2025; Chen et al., 2025), and different network components exhibit highly heterogeneous response behaviors with respect to varying input latent. As illustrated in Figure 4(b), we observed a clear disparity in activation variability across layers. As a result, applying uniformly quantization method on all network component is a suboptimal method for output quality.

To address this issue, we propose to allocate optimization effort according to each layer’s sensitivity to input variations. Specifically, we introduce **Variance-Oriented Layer Training Strategy (VOLTS)**, which reallocates layer-wise training budgets based on activation statistics, without modifying the model architecture or loss function.

VOLTS consists of a calibration phase followed by variance-guided training budget allocation as shown in Fig 3(b):

**Step 1: Layer Statistics Extraction.** Inspired by SmoothQuant (Xiao et al., 2023) and ViDiT-Q (Zhao et al., 2025), for each linear layer  $l$ , we collect its input activation  $\mathbf{X}^l \in \mathbb{R}^{B \times N \times C}$ , then we compute its channel-wise mean as a compact representation of the layer-level activation drift:

$$\mu^l(\mathbf{X}) = \frac{1}{C} \sum_{i=1}^C \mathbf{X}_{:, :, i}^l, \quad (5)$$

Compared to extreme-value statistics, the channel mean better reflects semantic-level representation changes while being robust to outliers, which is a better estimation metric.

**Step 2: Layer sensitivity estimation.** Using a calibration dataset  $\mathcal{D}_{\text{calib}}$ , we estimate the variance

$$\sigma_l^2 = \text{Var}_{\mathbf{X} \sim \mathcal{D}_{\text{calib}}}(\mu^l(\mathbf{X})), \quad (6)$$

for each layer. This variance measures how strongly a layer’s representation responds to different inputs. Layers with higher variance are more sensitive to data distribution changes and are therefore more vulnerable to quantization-induced errors, which needs more training resources.

**Step 3: Variance-guided training budget allocation.** Based on two thresholds  $\delta_1$  and  $\delta_2$ , layers are categorized into three groups for different training strategy:

- $\sigma_l^2 \in [0, \delta_1]$ : Low-variance layers, whose representations remain nearly invariant across inputs, are **frozen** after quantization layer initialization during training to avoid unnecessary disturbance.
- $\sigma_l^2 \in [\delta_1, \delta_2]$ : Medium-variance layers are assigned limited training process for **light adaptation**.
- $\sigma_l^2 \in [\delta_2, +\infty]$ : High-variance layers, exhibiting substantial input-dependent changes, are **optimized** until convergence to compensate for quantization errors.

By reallocating training budgets toward variance-sensitive layers, VOLTS prioritizes perceptually critical components of the network. In one-step diffusion models, variance-guided layer-wise adaptation shows particularly effectiveness because minimizing global quantization error does not necessarily correlate with perceptual quality.

### 3.5. Quantization-Aware Alternating Optimization

In low-bit quantization scenarios, the limited numerical precision are used to represent floating-point weights and activations, which inevitably leads to performance degradation. To mitigate the gap, a widely adopted strategy is to introduce a high-precision branch alongside the quantized branch (He et al., 2024; Li et al., 2025a; Fu et al., 2025). However, these two branches are often strongly coupled and have nearly identical influence on the final output. Merely enhancing the high-precision branch can inadvertently degrade the performance of the low-bit branch, and vice versa. This strong coupling necessitates a more principled joint optimization strategy that accounts for quantization constraints.

To address with these issues, we propose **Quantization-aware Alternating Optimization (QAO)**. We formulate

the quantization objective as follows:

$$\min_{\mathbf{L}_1, \mathbf{L}_2} \|(\hat{\mathbf{W}} - \mathbf{L}_1 \mathbf{L}_2) - \mathbf{Q}_W (\hat{\mathbf{W}} - \mathbf{L}_1 \mathbf{L}_2)\|_F \quad (7)$$

Here, the low-rank branch is optimized to approximate the quantization-compensated residual, rather than the original weight tensor directly. When training from scratch, the overall loss converges slowly. Moreover, if we apply the straight-through estimator (STE) gradient

$$\frac{\partial Q(x)}{\partial x} = \mathbf{1}[x \in [l, u]], \quad (8)$$

the gradient can vanish when  $\hat{\mathbf{W}} - \mathbf{L}_1 \mathbf{L}_2$  becomes sufficiently small, halting further optimization. Inspired by SVDQuant, we first perform singular value decomposition (SVD) on  $\hat{\mathbf{W}}$  to obtain a strong initialization for the low-rank parameters and fix quantization parameters, thereby avoiding repeated searches for optimal quantization scales. While this provides a favorable starting point, both SVD and quantization introduce inevitable approximation errors. Focusing solely on minimizing one type of error tends to yield suboptimal solutions in the quantized latent space. As outlined in Algorithm 1, we reduce quantization error by iteratively computing the residual  $\hat{\mathbf{W}} - \mathbf{Q}_W (\hat{\mathbf{W}} - \mathbf{L}_1 \mathbf{L}_2)$  and adjusting  $\mathbf{L}_1$  and  $\mathbf{L}_2$  over several iterations, finally selecting the parameters that achieve the minimal loss.

#### Algorithm 1 Quantization-Aware Alternating Optimization

```

1: Input: Layer weight  $\mathbf{W}$ , rank  $r$ , iteration rounds  $n$ 
2:  $\hat{\mathbf{W}} \leftarrow \mathbf{W}\mathbf{H}$ 
3:  $[\mathbf{U}, \Sigma, \mathbf{V}] \leftarrow \text{SVD}(\hat{\mathbf{W}})$ 
4:  $\mathbf{L}_1 \leftarrow \mathbf{U}\Sigma_{:, :r}, \mathbf{L}_2 \leftarrow \mathbf{V}_{:, r,:}$ 
5:  $\mathbf{R} \leftarrow \hat{\mathbf{W}} - \mathbf{L}_1 \mathbf{L}_2, \mathbf{W}_R \leftarrow \mathbf{Q}_W(\mathbf{R})$ 
6:  $Err^* \leftarrow +\infty$ 
7:  $\mathbf{L}_1^* \leftarrow \emptyset, \mathbf{L}_2^* \leftarrow \emptyset$ 
8: for  $i = 1$  to  $n$  do
9:    $err \leftarrow \|\mathbf{R} - \mathbf{W}_R\|_F$ 
10:  if  $err < Err^*$  then
11:     $Err^* \leftarrow err$ 
12:     $\mathbf{L}_1^* \leftarrow \mathbf{L}_1, \mathbf{L}_2^* \leftarrow \mathbf{L}_2$ 
13:  end if
14:   $[\mathbf{U}, \Sigma, \mathbf{V}] \leftarrow \text{SVD}(\hat{\mathbf{W}} - \mathbf{W}_R)$ 
15:   $\mathbf{L}_1 \leftarrow \mathbf{U}\Sigma_{:, :r}, \mathbf{L}_2 \leftarrow \mathbf{V}_{:, r,:}$ 
16:   $\mathbf{R} \leftarrow \hat{\mathbf{W}} - \mathbf{L}_1 \mathbf{L}_2, \mathbf{W}_R \leftarrow \mathbf{Q}_W(\mathbf{R})$ 
17: end for
18: return  $\mathbf{W}_R, \mathbf{L}_1^*, \mathbf{L}_2^*$ 

```

## 4. Experiments

### 4.1. Experimental Settings

**Data construction.** We use HQ-VSR (Chen et al., 2025) dataset for both one-step model training and calibration process. In the calibration stage, we randomly sample 50 videos and run full inference process using the FP DiT model. Evaluation is conducted on synthetic and real-world

datasets. UDM10 (Tao et al., 2017) and REDS30 (Nah et al., 2019) encompass various degradation types, which are well synthetic datasets. We employ the MVSFR4x (Wang et al., 2023b) dataset as real-world evaluations.

**Evaluation Metrics.** We assess model performance using quality assessment metrics for image (IQA) and video (VQA). The reference-based IQA metrics we adopt contain DISTS (Ding et al., 2020), PSNR, SSIM (Wang et al., 2004) and LPIPS (Zhang et al., 2018). We also utilize MANIQA (Yang et al., 2022), CLIP-IQA (Wang et al., 2023a) and MUSIQ (Ke et al., 2021), considering their no-reference based application. For video quality assessment, we employ warping error  $E_{warp}^*$  (Lai et al., 2018) based on flows and DOVER (Wu et al., 2023).

**Implementation Details.** Following the training settings of DOVE (Chen et al., 2025), we trained an one-step inference version of WAN2.1 (Wan et al., 2025) as basic full-precision(FP) backbone. The hyperparameter  $\delta_1$  and  $\delta_2$  for VOLTS are set to 0.001 and 0.075. The number of iterations for frozen, light adaptation and fully optimized are respectively set to 1, 30 and  $+\infty$ . For weight quantization, we use a static asymmetric channel-wise quantizer. The rank for the SVD path is set to  $r = 32$ . We use PyTorch and a NVIDIA RTX A6000 GPU to build all experiments.

### 4.2. Comparison with State-of-the-Art Methods

We employ several quantization methods for approach comparison: MinMax (Jacob et al., 2018), SmoothQuant (Xiao et al., 2023), Quarot (Ashkboos et al., 2024), ViDiT-Q (Zhao et al., 2025), and SVDQuant (Li et al., 2025a). We perform the qualitative and quantitative results with comparison aspects. We also compute the compression ability of our quantized model compared with origin FP backbone to fully demonstrate our performance in low-bit quantization.

**Qualitative Results.** Tab 1 exhibits quantitative values and comparisons. Our method transcends prior approaches on almost every metric in 4-bit settings. Under 6-bit conditions, the quantization error is reduced, narrowing the gap in reconstruction quality among various methods. No-reference IQA and VQA metrics are more sensitive to subtle texture differences and stylistic shifts, thereby amplifying fluctuations in perceptual scores. Nevertheless, the consistent improvement of reference-based IQA metrics indicates that our method still has advantages in restoring real structural information and suppressing low-bit quantization distortion.

**Visual Results.** Figs. 5 and 6 present visual comparisons. Compared to prior quantization approaches, LSGQuant produces more faithful textures and clearer details, with minimal difference from the FP model. When applied to Diffusion Transformer, previous leading quantization methods could generate impractical artifacts (e.g., SVDQuant on REDS30: 003), while our LSGQuant alleviates these distor-

## LSGQuant: Layer-Sensitivity Guided Quantization for One-Step Diffusion Real-World Video Super-Resolution

Table 1. Synthetic and real-world quantitative results. WAN stands for our one-step inference version for VSR tasks based on training settings of DOVE(Chen et al., 2025),with pretrained WAN2.1 (Wan et al., 2025) as our FP backbone components. Red and Blue texts represent the best and second best scores, respectively. LSGQuant shows leading metric performance on 4-bit scenarios.

Dataset	Bit	Method	PSNR↑	SSIM↑	LPIPS↓	DISTS↓	CLIP-IQA↑	MUSIQ↑	MANIQA↑	DOVER↑	$E_{warp}^* \downarrow$
UDM10	W6A6	W16A16   WAN (Wan et al., 2025)	23.74	0.7144	0.2886	0.2080	0.4973	63.85	0.3482	0.5494	0.93
		MinMax (Jacob et al., 2018)	23.27	0.7090	0.2987	0.2154	0.5205	63.73	0.3412	0.5135	0.95
		SmoothQuant (Xiao et al., 2023)	23.02	0.7014	0.3011	0.2180	0.5237	64.39	0.3520	0.5579	0.89
		QuaRot (Ashkboos et al., 2024)	23.66	0.7128	0.2912	0.2120	0.4990	63.78	0.3491	0.5403	0.92
		ViDiT-Q (Zhao et al., 2025)	23.08	0.7024	0.3005	0.2167	0.5224	64.38	0.3499	0.5513	0.86
		SVDQuant (Li et al., 2025a)	23.71	0.7125	0.2906	0.2101	0.4931	63.50	0.3441	0.5342	0.95
	W4A4	LSGQuant (ours)	23.69	0.7126	0.2911	0.2096	0.5028	64.00	0.3486	0.5441	0.94
		MinMax (Jacob et al., 2018)	19.68	0.6200	0.5789	0.4482	0.2568	28.97	0.2078	0.0448	2.12
		SmoothQuant (Xiao et al., 2023)	20.60	0.6288	0.5372	0.4233	0.2596	32.29	0.2189	0.0446	2.24
		QuaRot (Ashkboos et al., 2024)	22.72	0.6941	0.3489	0.2672	0.4346	56.90	0.2775	0.3436	1.36
		ViDiT-Q (Zhao et al., 2025)	21.89	0.6570	0.5052	0.4012	0.2565	25.72	0.1962	0.0559	1.36
		SVDQuant (Li et al., 2025a)	21.92	0.6544	0.4770	0.3781	0.5007	46.48	0.2768	0.1718	1.23
REDS30	W6A6	LSGQuant (ours)	23.80	0.7130	0.3169	0.2348	0.4966	59.15	0.3139	0.4333	1.07
		W16A16   WAN (Wan et al., 2025)	19.42	0.5145	0.3182	0.2479	0.3256	61.86	0.2889	0.4073	2.23
		MinMax (Jacob et al., 2018)	19.14	0.5129	0.3412	0.2653	0.3082	60.22	0.2784	0.3715	2.17
		SmoothQuant (Xiao et al., 2023)	19.03	0.5087	0.3379	0.2645	0.3179	61.71	0.2866	0.3975	2.07
		QuaRot (Ashkboos et al., 2024)	19.36	0.5152	0.3269	0.2551	0.3226	61.29	0.2866	0.3910	2.11
		ViDiT-Q (Zhao et al., 2025)	19.14	0.5100	0.3399	0.2667	0.3155	61.26	0.2831	0.3897	1.96
	W4A4	SVDQuant (Li et al., 2025a)	19.39	0.5134	0.3220	0.2494	0.3271	61.23	0.2862	0.3930	2.29
		LSGQuant (ours)	19.37	0.5128	0.3197	0.2491	0.3332	61.82	0.2884	0.4006	2.31
		MinMax (Jacob et al., 2018)	18.16	0.4595	0.6475	0.4835	0.2442	28.55	0.2204	0.0500	4.62
		SmoothQuant (Xiao et al., 2023)	18.74	0.4706	0.6161	0.4844	0.2726	28.81	0.2113	0.0468	4.44
		QuaRot (Ashkboos et al., 2024)	18.65	0.4921	0.4354	0.3445	0.2990	50.88	0.2368	0.2081	3.23
		ViDiT-Q (Zhao et al., 2025)	19.15	0.4830	0.5990	0.4607	0.2363	24.57	0.2085	0.0463	3.81
MVS4x	W6A6	SVDQuant (Li et al., 2025a)	18.70	0.4841	0.5387	0.4446	0.3535	32.61	0.2390	0.1022	2.70
		LSGQuant (ours)	19.72	0.5138	0.3671	0.2822	0.3067	54.31	0.2521	0.2967	2.73
		W16A16   WAN (Wan et al., 2025)	22.80	0.7434	0.3353	0.2661	0.4794	63.49	0.3904	0.5020	0.46
		MinMax (Jacob et al., 2018)	22.68	0.7460	0.3373	0.2712	0.4878	62.79	0.3771	0.4606	0.43
		SmoothQuant (Xiao et al., 2023)	22.56	0.7438	0.3374	0.2724	0.4870	63.13	0.3885	0.4915	0.41
		QuaRot (Ashkboos et al., 2024)	22.75	0.7438	0.3401	0.2693	0.4759	63.47	0.3907	0.4911	0.44
	W4A4	ViDiT-Q (Zhao et al., 2025)	22.56	0.7435	0.3365	0.2740	0.4811	62.92	0.3851	0.4939	0.39
		SVDQuant (Li et al., 2025a)	22.79	0.7419	0.3374	0.2689	0.4778	63.62	0.3893	0.4957	0.47
		LSGQuant (ours)	22.79	0.7420	0.3337	0.2655	0.4790	63.74	0.3903	0.5072	0.47
		MinMax (Jacob et al., 2018)	20.89	0.7139	0.5288	0.4203	0.2549	25.35	0.3416	0.0661	1.07
		SmoothQuant (Xiao et al., 2023)	21.05	0.7226	0.4934	0.4091	0.2728	28.73	0.2261	0.0891	0.95
		QuaRot (Ashkboos et al., 2024)	22.37	0.7422	0.3773	0.2990	0.4121	56.70	0.2988	0.3357	0.75
MVS4x	W4A4	ViDiT-Q (Zhao et al., 2025)	21.06	0.7351	0.4613	0.3877	0.2997	26.34	0.2307	0.1046	0.63
		SVDQuant (Li et al., 2025a)	21.69	0.7289	0.4559	0.3780	0.4141	39.80	0.2717	0.1615	0.62
		LSGQuant (ours)	22.82	0.7492	0.3317	0.2715	0.4543	58.90	0.3529	0.4257	0.52

Table 2. A comparison of Params, Ops, and compression ratios (DiT module only) across various quantization configurations. We input a latent input size of 16×9×90×158 for ops collection, which represents a 32×3×180×318 video in UDM10.

Method	Bits	Params / M (↓ Ratio)	Ops / G (↓ Ratio)
WAN2.1	W16A16	1419 (↓0%)	40110 (↓0%)
LSGQuant	W8A8	766 (↓45.97%)	21284 (↓46.94%)
LSGQuant	W6A6	592 (↓58.23%)	16274 (↓59.43%)
LSGQuant	W4A4	419 (↓70.49%)	11264 (↓71.92%)

tions. Moreover, due to the special design of the activation quantizer, LSGQuant has higher temporal consistency and better dynamic continuity. This is attributed to the combined effects of different mechanisms designed in the both inference process and training strategy.

**Compression Ability.** Following previous work (Qin et al., 2023), we report parameters (Params/M) and computational complexity (Ops/G) to demonstrate compression ratio. As shown in Table 2, versus the FP backbone, 6-bit LSGQuant reduces module params and computing by 58.08% and 59.43%, while 4-bit cuts them by 70.34% and 71.92%.

These results fully demonstrates the compression capability and deployment potential of our method.

### 4.3. Ablation Study

**Dynamic-Range Adaptive Activation Quantizer (DRAQ).** We conduct experiments under three activation quantization settings: (1) a baseline per-token symmetric quantizer without channel-wise range adaptation; (2) a static channel-wise quantizer that uses fixed ranges, determined by collecting per-channel absolute maximum values from the calibration dataset concurrently with Step 1 of VOLTS; and (3) our proposed DRAQ. As shown in Tab. 3a, DRAQ yields significant performance gains compared to the other two settings. Specifically, the performance drops significantly if the scaling factor is replaced with data determined in setting (2), which further demonstrates that calibration data fails to capture the complete input dynamic range. So applying a flexible and dynamic activation quantization strategy is significant for minimizing quantization error. These experiments evaluate the effectiveness of DRAQ.



Figure 5. We conduct 4-bit scenarios visual exhibition for synthetic (REDS30 (Nah et al., 2019)) and real-world (MVS4x (Wang et al., 2023b)) datasets. In 4-bit settings, our approach significantly surpasses recent existing methods.

Table 3. Ablation study on different method settings. Experiments are conducted on UDM10 (Tao et al., 2017) with W4A4 quantization.

(a) Activation quantizer scaling calculation.

Method	No scaling	Calibrated Scaling	DRAQ
PSNR $\uparrow$	23.72	20.04	<b>23.80</b>
DISTS $\downarrow$	0.2380	0.4352	<b>0.2348</b>
CLIP-IQA $\uparrow$	0.4855	0.2450	<b>0.4966</b>
DOVER $\uparrow$	0.3996	0.0231	<b>0.4333</b>

(b) Weight quantization algorithms.

Method	No QAO	With QAO
PSNR $\uparrow$	23.23	<b>23.80</b>
DISTS $\downarrow$	0.2582	<b>0.2348</b>
CLIP-IQA $\uparrow$	0.4650	<b>0.4966</b>
DOVER $\uparrow$	0.4162	<b>0.4333</b>

(c) Layer sensitivity estimation scheme.

Sensitivity estimation levels	Uniform		Simplified		Ours
	Lightly Adapted	Fully Optimized	Frozen + Lightly Adapted	Frozen + Fully Optimized	
PSNR $\uparrow$	23.74	23.43	23.75	23.52	<b>23.80</b>
DISTS $\downarrow$	0.2351	0.2424	0.2349	0.2395	<b>0.2348</b>
CLIP-IQA $\uparrow$	0.4966	0.4801	0.4901	0.4848	<b>0.4966</b>
DOVER $\uparrow$	0.4328	0.4211	0.4395	<b>0.4571</b>	0.4333



Figure 6. Temporal consistency exhibition (by tracking the line across videos). Our method achieves better spatial and temporal consistency than compared approaches.

**Variance-Oriented Training Strategy (VOLTS).** We allocate varying numbers of training iterations based on different layer sensitivity estimation schemes: (1) a uniform scheme where all trainable layers are treated equally as either lightly-adapted or fully-optimized; (2) a simplified scheme where unfrozen layers are treated identically; and (3) our proposed scheme featuring a three-tier classification. Results in Table 3c confirm that the proposed classification strategy achieves better performance, and it is significant for reasonably defining the importance and sensitivity of different types of layers in the diffusion transformer module, especially in a one-step inference scenario.

**Quantization Aware Optimization (QAO).** We compare the model performance with and without the proposed quantization-aware alternating optimization. As demonstrated in Table 3b, the QAO strategy leads to clearly better results, which proves that it is essential to jointly optimize the quantized and high-precision branches and get better output quality. Additionally, the iterative approach has better output video quality and minor weight quantization error.

## 5. Conclusion

We introduce LSGQuant in this article, an approach for video super-resolution tasks relying one-step diffusion and its low-bit quantization. To effectively handle video tokens, we introduce a Dynamic-Range Adaptive Quantizer (DRAQ), which significantly mitigates activation quantization errors. Furthermore, we design a Variance-Oriented Layer Training Strategy (VOLTS) and a Quantization-Aware Alternating Optimization (QAO) scheme under strict one-step inference constraints. Extensive testing results prove that LSGQuant achieves competitive output video quality compared to full-precision baselines and has practical value.

## References

Ashkboos, S., Mohtashami, A., Croci, M. L., Li, B., Cameron, P., Jaggi, M., Alistarh, D., Hoefler, T., and Hensman, J. Quarot: Outlier-free 4-bit inference in rotated llms. In *NeurIPS*, 2024.

Blattmann, A., Dockhorn, T., Kulal, S., Mendelevitch, D., Kilian, M., Lorenz, D., Levi, Y., English, Z., Voleti, V., Letts, A., et al. Stable video diffusion: Scaling latent video diffusion models to large datasets. *arXiv preprint arXiv:2311.15127*, 2023.

Chan, K. C., Wang, X., Yu, K., Dong, C., and Loy, C. C. Basicvsr: The search for essential components in video super-resolution and beyond. In *CVPR*, 2021.

Chan, K. C., Zhou, S., Xu, X., and Loy, C. C. Basicvsr++: Improving video super-resolution with enhanced propagation and alignment. In *CVPR*, 2022.

Chen, H., Zhang, Y., Cun, X., Xia, M., Wang, X., Weng, C., and Shan, Y. Videocrafter2: Overcoming data limitations for high-quality video diffusion models. In *CVPR*, 2024.

Chen, Z., Zou, Z., Zhang, K., Su, X., Yuan, X., Guo, Y., and Zhang, Y. Dove: Efficient one-step diffusion model for real-world video super-resolution. In *NeurIPS*, 2025.

Ding, K., Ma, K., Wang, S., and Simoncelli, E. P. Image quality assessment: Unifying structure and texture similarity. *TPAMI*, 2020.

Dong, L., Fan, Q., Guo, Y., Wang, Z., Zhang, Q., Chen, J., Luo, Y., and Zou, C. Tsd-sr: One-step diffusion with target score distillation for real-world image super-resolution. *CVPR*, 2025.

Fu, M., Yu, H., Shao, J., Zhou, J., Zhu, K., and Wu, J. Quantization without tears. In *CVPR*, 2025.

He, Y., Liu, J., Wu, W., Zhou, H., and Zhuang, B. Efficientdm: Efficient quantization-aware fine-tuning of low-bit diffusion models. *ICLR*, 2024.

Ho, J., Jain, A., and Abbeel, P. Denoising diffusion probabilistic models. In *NeurIPS*, 2020.

Jacob, B., Kligys, S., Chen, B., Zhu, M., Tang, M., Howard, A., Adam, H., and Kalenichenko, D. Quantization and training of neural networks for efficient integer-arithmetic-only inference. In *CVPR*, 2018.

Jo, Y., Oh, S. W., Kang, J., and Kim, S. J. Deep video super-resolution network using dynamic upsampling filters without explicit motion compensation. In *CVPR*, 2018.

Ke, J., Wang, Q., Wang, Y., Milanfar, P., and Yang, F. Musiq: Multi-scale image quality transformer. In *ICCV*, 2021.

Lai, W.-S., Huang, J.-B., Wang, O., Shechtman, E., Yumer, E., and Yang, M.-H. Learning blind video temporal consistency. In *ECCV*, 2018.

Li, M., Lin, Y., Zhang, Z., Cai, T., Li, X., Guo, J., Xie, E., Meng, C., Zhu, J.-Y., and Han, S. Svdquant: Absorbing outliers by low-rank components for 4-bit diffusion models. In *ICLR*, 2025a.

Li, X., Liu, Y., Cao, S., Chen, Z., Zhuang, S., Chen, X., He, Y., Wang, Y., and Qiao, Y. Diffvsr: Revealing an effective recipe for taming robust video super-resolution against complex degradations. *ICCV*, 2025b.

Liang, J., Cao, J., Fan, Y., Zhang, K., Ranjan, R., Li, Y., Timofte, R., and Van Gool, L. Vrt: A video restoration transformer. *TIP*, 2024.

Liu, Z., Zhao, C., Fedorov, I., Soran, B., Choudhary, D., Krishnamoorthi, R., Chandra, V., Tian, Y., and Blankevoort, T. Spinquant: Llm quantization with learned rotations. *ICLR*, 2025.

Nah, S., Baik, S., Hong, S., Moon, G., Son, S., Timofte, R., and Mu Lee, K. Ntire 2019 challenge on video deblurring and super-resolution: Dataset and study. In *CVPRW*, 2019.

Qin, H., Zhang, Y., Ding, Y., Liu, X., Danelljan, M., Yu, F., et al. Quantsr: accurate low-bit quantization for efficient image super-resolution. In *NeurIPS*, 2023.

Ramesh, A., Dhariwal, P., Nichol, A., Chu, C., and Chen, M. Hierarchical text-conditional image generation with clip latents. *arXiv preprint arXiv:2204.06125*, 2022.

Rombach, R., Blattmann, A., Lorenz, D., Esser, P., and Ommer, B. High-resolution image synthesis with latent diffusion models. In *CVPR*, 2022.

Shang, Y., Yuan, Z., Xie, B., Wu, B., and Yan, Y. Post-training quantization on diffusion models. In *CVPR*, 2023.

Tao, X., Gao, H., Liao, R., Wang, J., and Jia, J. Detail-revealing deep video super-resolution. In *ICCV*, 2017.

Wan, T., Wang, A., Ai, B., Wen, B., Mao, C., Xie, C.-W., Chen, D., Yu, F., Zhao, H., Yang, J., et al. Wan: Open and advanced large-scale video generative models. *arXiv preprint arXiv:2503.20314*, 2025.

Wang, J., Chan, K. C., and Loy, C. C. Exploring clip for assessing the look and feel of images. In *AAAI*, 2023a.

Wang, J., Lin, Z., Wei, M., Zhao, Y., Yang, C., Xiao, F., Loy, C. C., and Jiang, L. Seedvр: Seeding infinity in diffusion transformer towards generic video restoration. In *CVPR*, 2025.

Wang, R., Liu, X., Zhang, Z., Wu, X., Feng, C.-M., Zhang, L., and Zuo, W. Benchmark dataset and effective inter-frame alignment for real-world video super-resolution. In *CVPRW*, 2023b.

Wang, Y., Yang, W., Chen, X., Wang, Y., Guo, L., Chau, L.-P., Liu, Z., Qiao, Y., Kot, A. C., and Wen, B. Sinsr: diffusion-based image super-resolution in a single step. In *CVPR*, 2024.

Wang, Z., Bovik, A. C., Sheikh, H. R., and Simoncelli, E. P. Image quality assessment: from error visibility to structural similarity. *TIP*, 2004.

Wang, Z., Lu, C., Wang, Y., Bao, F., Li, C., Su, H., and Zhu, J. Prolificdreamer: High-fidelity and diverse text-to-3d generation with variational score distillation. In *NeurIPS*, 2023c.

Wu, H., Zhang, E., Liao, L., Chen, C., Hou, J., Wang, A., Sun, W., Yan, Q., and Lin, W. Exploring video quality assessment on user generated contents from aesthetic and technical perspectives. In *ICCV*, 2023.

Wu, J., Wang, H., Shang, Y., Shah, M., and Yan, Y. Ptq4dit: Post-training quantization for diffusion transformers. *NeurIPS*, 2024a.

Wu, R., Sun, L., Ma, Z., and Zhang, L. One-step effective diffusion network for real-world image super-resolution. In *NeurIPS*, 2024b.

Xiao, G., Lin, J., Seznec, M., Wu, H., Demouth, J., and Han, S. Smoothquant: Accurate and efficient post-training quantization for large language models. In *ICML*, 2023.

Xie, R., Liu, Y., Zhou, P., Zhao, C., Zhou, J., Zhang, K., Zhang, Z., Yang, J., Yang, Z., and Tai, Y. Star: Spatial-temporal augmentation with text-to-video models for real-world video super-resolution. *arXiv preprint arXiv:2501.02976*, 2025.

Yang, S., Wu, T., Shi, S., Lao, S., Gong, Y., Cao, M., Wang, J., and Yang, Y. Maniq: Multi-dimension attention network for no-reference image quality assessment. In *CVPRW*, 2022.

Yang, Z., Teng, J., Zheng, W., Ding, M., Huang, S., Xu, J., Yang, Y., Hong, W., Zhang, X., Feng, G., et al. Cogvideox: Text-to-video diffusion models with an expert transformer. In *ICLR*, 2025.

Zhang, R., Isola, P., Efros, A. A., Shechtman, E., and Wang, O. The unreasonable effectiveness of deep features as a perceptual metric. In *CVPR*, 2018.

Zhao, T., Fang, T., Huang, H., Liu, E., Wan, R., Soedarmadji, W., Li, S., Lin, Z., Dai, G., Yan, S., et al. Vudit-q: Efficient and accurate quantization of diffusion transformers for image and video generation. *ICLR*, 2025.

Zhou, S., Yang, P., Wang, J., Luo, Y., and Loy, C. C. Upscale-a-video: Temporal-consistent diffusion model for real-world video super-resolution. In *CVPR*, 2024.

Zhu, L., Li, J., Qin, H., Li, W., Zhang, Y., Guo, Y., and Yang, X. Passionsr: Post-training quantization with adaptive scale in one-step diffusion based image super-resolution. In *CVPR*, 2025.